Controlled reversible aggregation of thermoresponsive polymeric nanoparticles by interfacial Diels-Alder reaction

Madeline Vauthier, Christophe Serra

Controlled Reversible Aggregation of Thermoresponsive Polymeric Nanoparticles by Interfacial Diels-Alder Reaction

Madeline Vauthier,[†*] Christophe A. Serra[†]

† Université de Strasbourg, CNRS, Institut Charles Sadron UPR 22, F-67000 Strasbourg, France
Email: madeline.vauthier@ics-cnrs.unistra.fr, ca.serra@unistra.fr
Corresponding author: Dr. M. Vauthier, +33(0)388 414 194

ABSTRACT:

Hypothesis:

Stimuli-responsive polymers, with properties changing upon different environmental factor variations such as pH, light, mechanical stress or temperature, and polymeric nanoparticles have found many important applications in fields such as drug delivery, biosensing and environmental research.

Experiments:

In this work, thermoresponsive nanoparticles that are able to react by Diels-Alder reaction (a diene-dienophile cycloaddition) were studied. Thermoresponsive polymers were synthesized from a biocompatible polymer (poly(lactic-co-glycolic) acid, PLGA) and diene (furan) or dienophile (maleimide) derivatives. Emulsification-evaporation method was then used as a fast and reproducible method to obtain highly monodispersed polymeric nanosuspensions able to react by Diels-Alder (DA) reaction.

Findings:

The nanoparticles' size decreased down to 25 nm by increasing the emulsification's time. The possible direct and retro-Diels-Alder (rDA) reactions between furan- and maleimide-functionalized nanoparticles were studied by dynamic light scattering and electron microscopy. For the first time, the reactivity of the interfacial DA and rDA reactions between functionalized-nanoparticles was studied, leading to the determination of the activation energy, the enthalpy of activation and the entropy of activation.

KEY WORDS: thermoresponsive polymers, nanoparticles, thermorelease, smart materials, interfacial Diels-Alder reaction

I. INTRODUCTION

The number of studies aiming at designing new smart materials keeps increasing since the beginning of 20th century because they play an important role in the development of new advanced technologies. [1–3] Today, we can find smart materials in all areas of activity. [4–6] Recently, chemical stimuli have been studied for various applications, such as the production of pH-responsive materials to control drug delivery and separation processes. [7,8] The presence of specific molecules, containing polar groups or able to form hydrogen bonds for instance, can also modify the properties of materials. [9–12] Besides, physical stimuli have also gained a lot of interest because they can be remotely applied. Indeed, electro- or magneto-active materials can be used to elaborate sensors or robotic muscles for instance. [13–16] Photo-sensitive polymers can change their properties in response to light irradiation at a given wavelength and intensity. They are broadly used for bio-patterning and photo-triggered drug delivery. [16] Another highly-studied physical stimulus consists in the variation of the environmental temperature. This method is used to elaborate self-healing materials (composites) thanks to weak (H-bonds) or covalent interactions. [17–20] In this study, we are especially interested in smart materials that respond to a thermal stimulus. Few reactions can actually be classified as thermoreversible reactions, in the sense that they lead to the formation of covalent bonds that are reversible only *via* a thermal stimulus. To the best of our knowledge, they concern alkoxylamine bonds, [21,22] the reversible formation of thiazolinediones[23] and the formation of Diels-Alder adducts. [24,25] The latter reaction, classified as a click-reaction, [26,27] corresponds to the cycloaddition between a 1.3 conjugated-diene and a dienophile (a molecule containing a double or triple bond) [24] and is the most studied. This reaction is the topic of this study: since most of thermosensitive particles presented in the literature were made from chitosan derivatives or poly(N-isopropylacrylamide), [28–32] we prove that the Diels-Alder (DA) chemistry can also be applied to obtain thermoresponsive nanoparticles (NPs). The DA reaction is facilitated when the energetic gap between the electronic orbitals of the diene (HOMO) and the dienophile (LUMO) are low and, thus, it decreases the reaction temperature and time.[24] Furan-maleimide pair has a low HOMO/LUMO gap and this is why it was mainly studied in the literature.[25,33–37] We thus first investigated the reactivity of nanoparticles produced from furan- and maleimide-functionalized poly(lactic-co-glycolic) acid (PLGA), a biocompatible polymer allowing us to target a wide range of applications, and the reversibility of the DA reaction. Indeed, the interfacial retro-Diels-Alder (rDA) reaction has been less studied than the direct DA reaction[34,37] and has never been studied yet at the surface of polymeric particles. The main advantages of this work are i) to not depend on inorganic materials that are potentially toxic and rarely degradable, ii) to work with few amounts of chemicals (more economically viable) and iii) to be able to reach a wide range of nanoparticles' size by tuning the process parameters.

II. MATERIALS AND METHODS

II.1. Materials

N-(2-Aminoethyl)maleimide was obtained from *N*-(2-Aminoethyl)maleimide trifluoroacetate salt (Sigma) by liquid-liquid extraction.

Poly(lactic-co-glycolic acid) 50:50 (PLGA) (Resomer® RG504 H, Sigma, 60 kg mol^{-1}) was functionalized by furfurylamine (Sigma) and *N*-(2-Aminoethyl)maleimide (Sigma) in order to obtain furan- and maleimide-derivatives. Dicyclohexylcarbodiimide (DCC, Alfa Aesar) and N-Hydroxysuccinimide (NHS, Sigma) were used to activate the PLGA. Dichloromethane (DCM, Sigma), ethyl acetate (Sigma) and surfactant (Pluronic® F-127, Sigma) were used as received.

II.2. Preparation of thermoresponsive polymers

Furan- and maleimide-functionalized PLGA, represented in Figure 1, were prepared by adapting the method of Dinarvand's team. [40] 1 g of PLGA dissolved in DCM was activated by 70 mg of DCC and 49 mg of NHS at room temperature for 24 h. The resultant solution was precipitated by dropping into ice-cold diethyl ether, filtered and dried under vacuum. The activated PLGA (0.5 g) dissolved in 5 mL of DCM was added to 1 mg of furfurylamine (or 1.5 mg of *N*-(2-aminoethyl)maleimide) dissolved in 1 mL of DCM. The reaction was carried out under stirring for 7 h at room temperature. The resultant solution was precipitated by dropping into ice-cold diethyl ether, filtered and dried under vacuum.

Furan-functionalized PLGA (Figure S1.a): ^{1}H NMR (400 MHz, $CDCl_3$): δ (ppm) 1.57 (m, 3 H), 4.28 (s, 2 H), 4.81 (m, 2 H), 5.21 (m, 1 H), 6.60 (t, *J = 3.5 Hz*, 1 H), 6.78 (t, *J = 4.0 Hz*, 1 H), 7.52 (s, 1 H).

The average molar masses of the furan-functionalized PLGA are Mn = 31.88 kg mol^{-1} and Mw = 63.72 kg mol^{-1} (Figure S2.a).

Maleimide-functionalized PLGA (Figure S1.b): ^{1}H NMR (400 MHz, $CDCl_3$): δ (ppm) 1.57 (m, 3 H), 2.65 (d, *J = 4.0 Hz*, 2 H), 4.11 (t, *J = 7.2 Hz*, 2 H), 4.81 (m, 2 H), 5.21 (m, 1 H), 7.38 (d, *J = 10.0 Hz*, 2 H).

The average molar masses of the maleimide-functionalized PLGA are Mn = 33.08 kg mol^{-1} and Mw = 64.24 kg mol^{-1} (Figure S2.b).

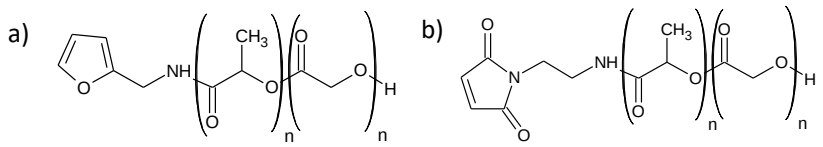

Figure 1. a) Furan- and b) maleimide-functionalized PLGA synthesized for this study.

II.3. Preparation of emulsions by elongational-flow micromixing process

The continuous phases were composed of 15 g L^{-1} of surfactant (Pluronic® F-127) solubilized in deionized water. The dispersed phases were composed of 2 g L^{-1} of polymer (furan-functionalized PLGA or maleimide-functionalized PLGA) solubilized in ethyl acetate (Sigma).

The continuous phase (15 v%) and the dispersed phase (85 v%) were used as the raw material for the emulsification system. It was mainly assembled with two mid-pressure syringe pumps (neMESYS® Mid Pressure Module, Cetoni) working in opposite phase (withdraw/infuse) and two 25 mL stainless steel syringes (Cetoni). This system was controlled by Cetoni's software to accurately operate flow rate (fixed at 30 mL min^{-1}). A back and forth movement of the pump counts for one cycle. The micromixer was fabricated such as to obtain three drilled cylindrical microchannels having a diameter of 150 µm, acting as a restriction to the flow, forming nanoemulsions by elongation process. Two microchannels were connected to the stainless-steel syringes with two PTFE tubes (1.06 mm ID x 1.68 mm OD) and the third microchannel was used to finally collect the emulsion. At the end of the process, the samples were collected, poured in a plastic vial and left overnight in a fume hood to let the organic solvent evaporated.

II.4. Characterization methods

II.4.1. Size-exclusion chromatography

Molecular weights and molecular weight distributions were determined using a SEC system equipped with a Shimadzu LC-20AD

pump, a Shimadzu SIL-20AHT automatic injector, a Shimadzu DGU-20A in-line deaerator, three PLgel B columns in row (separation: 500 g mol-1 – 10 Mg mol-1, 10 µm, 300 mm length x 7.5 mm ID) and a Shimatzu RID-10A refractive index detector. The measurements were operated at 30°C, thanks to a Shimadzu CTO-10AC oven, using toluene as eluent at a flow rate of 1 mL min-1 as using chloroform as flow marker. The molecular weight calibration was based on twelve narrow molecular weight linear polystyrene standards from Polymer Laboratories (molecular weights between 1,280 and 629,500 g mol-1).

II.4.2. Nuclear magnetic resonance spectroscopy

^{1}H NMR spectra were recorded on Bruker Advance DPX400 (400 MHz) spectrometer. The NMR chemical shifts were reported as the d scale in ppm relative to the solvent peak (d = 7.26) in $CDCl_3$. The terms m, s, d, t, q and dd represent multiplet, singlet, doublet, triplet, quadruplet and doublet of doublet respectively. Coupling constants (*J*) are given in Hertz (Hz).

II.4.3. Diameter and size distribution

The z-average diameter and the size distribution of the nanoparticles were based on "number value", assessed by dynamic light scattering (DLS) using a Nano ZetaSizer instrument (Malvern, France). The helium-neon laser (4 mW) was operated at 633 nm and the scatter angle was fixed at 173°. The samples' temperature was fixed between 289 K and 353 K, depending on the targeted reaction's temperature. The polydispersity index of the particle size (PDI) is a measure of the broadness of the size distribution and it is commonly admitted that PDI values below 0.2 corresponds to monomodal distributions. [41,42] Analyses of nanosuspensions size were performed by pouring dropwise 0.02 mL of the nanosuspensions into 1 mL of deionized water. Thirty measurements were conducted for each triplicate.

II.4.4. Transmission Electron Microscopy

To analyze the morphology and shape of the particles, cryo-transmission electron microscopy (cryo-TEM) experiments were performed. A 5 µL drop of the NPs suspension was deposited onto a lacey-holey carbon film (Ted Pella) freshly glow discharged (Elmo, Cordouan Technologies). The grid was frozen in liquid ethane cooled by liquid nitrogen in a home-made environment-controlled machine. The grids were mounted onto a Gatan 626 cryoholder and observed in a Tecnai G2 (FEI-Eindhoven) operating at 200 kV and the images were taken with an Eagle 2k2k ssCCD camera (FEI- Eindhoven) under low dose conditions.

III. RESULTS AND DISCUSSIONS

III.1. Production of biodegradable, thermoresponsive nanoparticles

In previous works, our team studied the influence of various process parameters on the polymeric (nano)particles size, leading to the conclusion that, in order to obtain small nanoparticles, the process time has to be long. [39,43, 44] These results were confirmed in this work with two nanoemulsions (Figure 2):

- FUR: with furan-functionalized PLGA in the dispersed phase
- MAL: with maleimide-functionalized PLGA in the dispersed phase

Indeed, increasing the elongational-flow micromixing time from 20 to 150 min decreased the average NPs size from 114 ± 8 nm to 27 ± 4 nm for FUR and from 121 ± 12 nm to 29 ± 4 nm for MAL. The PDI also decreased from 0.36 ± 0.05 to 0.11 ± 0.01 for FUR and from 0.24 ± 0.04 to 0.17 ± 0.01 for MAL.

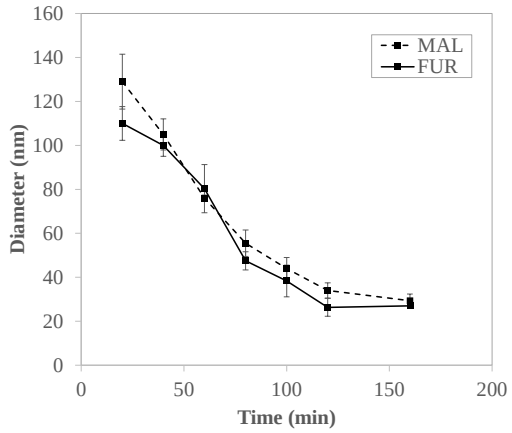

Figure 2. Evolution of FUR and MAL nanoparticles size regarding to the emulsification time at a constant flow rate of 30 mL min^{-1}.

III.2. Reversible aggregation of nanoparticles having the same size

After validating by SEC, in solution, the formation of the Diels-Alder (DA) adduct by reaction between the furan-functionalized PLGA and the maleimide-functionalized PLGA (Figure S2.c), the reversible adhesion by the DA and retro-DA (rDA) reactions between the previously produced polymeric nanoparticles (FUR and MAL) after 120 min of emulsification has been investigated (Figure 3). These nanoemulsions will be called FUR_120 and MAL_120 in the following study.

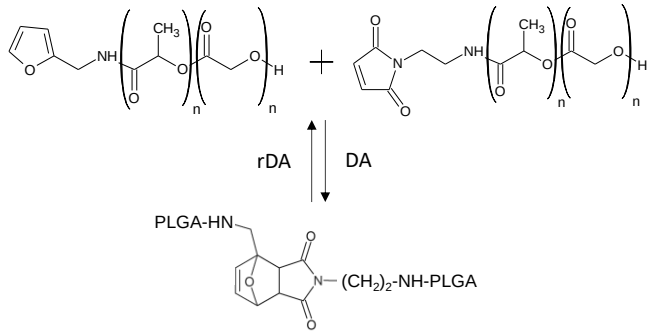

Figure 3. Diels-Alder and retro-Diels-Alder reactions that occur at the interface between FUR_120 and MAL_120 nanoparticles.

III.2.1. Reactivity study of the interfacial Diels-Alder reaction between nanoparticles

Roucoules' team previously proved that, on flat surfaces, the interfacial DA reaction with furan/maleimide pair occurred in less than five hours at room temperature due to the polymer chains confinement. [33] So, in this part the progress of the DA reaction between FUR_120 and MAL_120 nanoparticles has been investigated by measuring the size of the formed aggregates (FUR_120:MAL_120 ratio 1:1) since the formation of the adduct at the interface between co-NPs significantly increased the size measured by DLS. The evolution of the appearing diameter of the aggregates with the reaction time after mixing FUR_120 and MAL_120 at various temperatures (ranging from 288 K to 313 K) is reported in Figure 4. It is noteworthy that the diameter given by DLS was based on a hard sphere model but did not represent the actual shape of the aggregates.

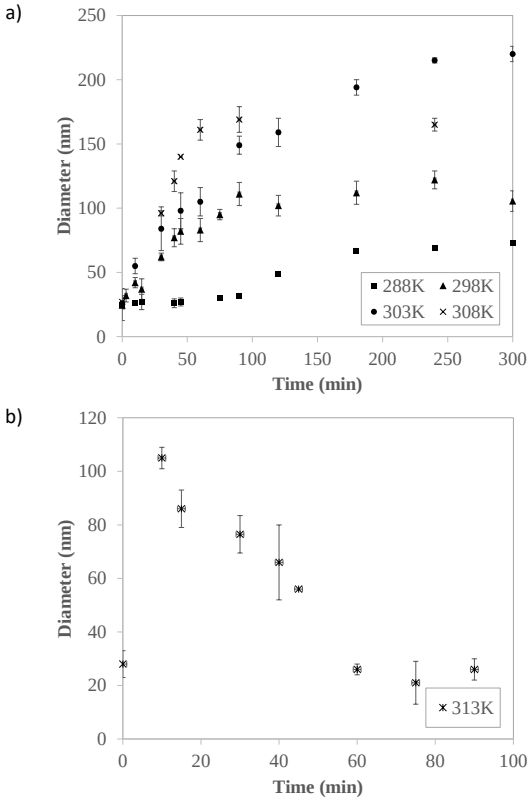

Figure 4. Evolution of the measured/appearing diameter regarding to time after mixing FUR_120 and MAL_120 in water at different temperatures a) below 313 K and b) at 313 K.

In Figure 4.a, after mixing FUR_120 and MAL_120 in water for 5 hours, the size measured by DLS reached 63 ± 6 nm at 288 K, 106 ± 8 nm at 298 K, 220 ± 6 nm at 303 K and 165 ± 5 nm at 308 K. These results proved that the DA reaction occurred at the interface between FUR_120 and MAL_120, leading to their aggregation below 313 K. It is noteworthy that the curves in Figure 4 suggested, for different temperatures, a different maximum number of particles per aggregate after 300 min of reaction. This most likely originated from the variation of reaction rates of the DA reaction with temperature. Indeed, all plateau values should be the same but were reached in a slower or faster manner depending in the reaction's temperature.

The rate law of this reaction is given in Equation 1. As a bimolecular reaction, and in accordance with the literature, the DA reaction had a second-order kinetics. [33,35,37] Moreover, it was assumed that the reversibility of this reaction can be neglected at the temperatures that have been tested (below 313 K):

$v = -d[FUR]/dt = k_{DA}[MAL][FUR]$ (1)

with k_{DA} the DA kinetic rate constant, [MAL] and [FUR] the surface content of dienophile and diene onto MAL_120 and FUR_120 NPs respectively (g L^{-1} nm^{-1}).

Since the grafting rate of furan- and maleimide-derivatives were the same (Table S1), and since FUR_120 and MAL_120 were introduced in the same quantity and in stoichiometric proportions, [MAL] = [FUR] at any time of the reaction. The rate law can thus be simplified as follows (Equation 2):

$v = k_{DA}[FUR]^2$ (2)

The surface density of the residual furan functions was related to the variation of the experimental size measurement. Indeed, the production of an adduct lead to the aggregation of nanoparticles. 1/[FUR] (second-order kinetics) was thus plotted versus the reaction time for the different temperatures and a linear dependence was observed (Figure S3), allowing the determination of DA rate constants, k_{DA} (Table 1).

Table 1. Values of Diels-Alder rate constants, k_{DA}, determined at different temperatures.

T (K)	288	298	303	308
k_{DA} x 10^2 (L g^{-1} nm s^{-1})	0.04	0.82	1.90	3.20

As expected, the values of k_{DA} increase with the reaction temperature. The slope of the linearization plot of Arrhenius equation (Equation 3, Figure S4) gave an estimation of the activation energy of this reaction Ea_{DA} = 166 ± 4 kJ mol^{-1}, which was higher than the interfacial DA reaction reported in the literature, between furan-functionalized flat surfaces and a maleimide-derivative in solution (E_a = 54 ± 6 kJ mol^{-1}). [33] Indeed, due to the NPs' Brownian motion, [45] the probability that the two reactants enter in contact to undergo the DA reaction was lower in our study.

$$k = Ae^{-\frac{Ea}{RT}} \quad (3)$$

with k the reaction rate constant, Ea the activation energy, R the perfect gas constant and T the medium temperature.

Moreover, the transition state theory enabled the calculation of thermodynamic parameters related to the formation of the transition state during the DA reaction between FUR_120 and MAL_120 thanks to Eyring equation (Equation 4, Figure S5): the enthalpy of activation was $\Delta H^{\neq}$ = 1.81 ± 0.03 kJ mol^{-1} and the entropy of activation $\Delta S^{\neq}$ was equal to -0.19 ± 0.01 kJ mol^{-1} K^{-1}. The positive value of $\Delta H^{\neq}$ evidenced that the DA reaction was endothermic. The value of $\Delta S^{\neq}$ shows that few increase of order occurred by the DA reaction, probably due to a decrease of Brownian motion by formation of aggregates.

$$k = \frac{k_B T}{h} e^{-\frac{(\Delta H^{\neq} - T\Delta S^{\neq})}{RT}} \quad (4)$$

with k the reaction rate constant, k_B the Boltzmann constant, h the Planck constant, T the medium temperature, R the perfect gas constant, $\Delta H^{\neq}$ the enthalpy of activation and $\Delta S^{\neq}$ the entropy of activation.

Interestingly, at 313 K the size increased (from 28 ± 5 nm to 105 ± 4 nm) before decreasing down to 26 ± 4 nm after 60 min (Figure 4.b). This effect was probably due to the retro-Diels-Alder (rDA) reaction that could not be neglected anymore above 313 K. The first increase was probably due to the preponderant DA reaction, forming the first aggregates, immediately followed by a partial rDA reaction.

III.2.2. Reversibility of the interfacial Diels-Alder reaction between nanoparticles

In order to confirm the previous assumption, to prove the reversibility of the particles' bonding and to demonstrate the chemical stability of the developed system, the rDA reaction was investigated before operating several DA/rDA cycles between NPs produced from furan- and maleimide-functionalized PLGA. In the literature, it has been proved that the interfacial rDA reaction could occur between 353 K and 430 K for the furan-maleimide pair. [33,37,46] Moreover, in the previous part, the rDA reaction seemed to start at 313 K In this study, the rDA reaction has thus been investigated between 313 K and 353 K (Figure 5), in order to avoid the degradation of PLGA due to heat.

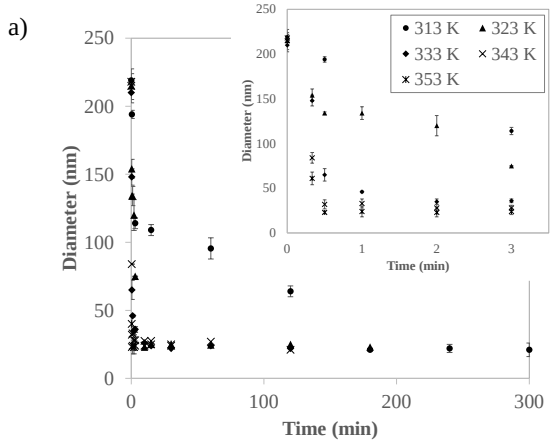

Figure 5. Evolution of the measured size a) regarding to time after heating the aggregated NPs *via* DA reaction at various temperatures and b) after various DA (298 K, 2 hrs) / rDA (323 K, 1 hr) cycles.

In Figure 5.a, the size measured by DLS decreased with heating time down to 22 ± 5 nm reaching pretty much the same size before heating (27 ± 4 nm, Figure 3). This suggests the disaggregation of the NPs aggregates due to their debonding. This proved that the rDA reaction occurred during that time. The plateau value around 22 nm demonstrated that the rDA reaction reached 100% yield at that time. The fact that the optimal rDA reaction temperature was low (323 K) may be due to the lower stability of the DA adduct between functional NPs than in solution or between furan-functionalized flat surfaces and a maleimide-derivative in solution.
Using the same thermodynamic method than developed previously, the retro-Diels-Alder rate constants, k_{rDA} (Equation 5), were determined at various temperatures (Table 2).

$$v = k_{rDA}[ADDUCT] \quad (5)$$

with k_{rDA} the rDA kinetic rate constant (s^{-1}) and [ADDUCT] the surface content of adduct (g L^{-1} nm^{-1}).

Table 2. Values of retro-Diels-Alder rate constants, k_{rDA}, determined at different temperatures.

T (K)	313*	323	333	343	353
k_{rDA} (s^{-1})	(0.25)	0.25	1.19	2.87	4.47

*The value at 313 K is given as an indication since the DA reaction cannot be completely neglected at that temperature.

The values of k_{rDA} increase with the reaction temperature and they obey the Arrhenius law (Figure S7), allowing the estimation of the activation energy of this reaction Ea_{rDA} = 8.2 ± 0.2 kJ mol^{-1}. This value was lower than the one from the interfacial DA reaction (Ea_{DA} = 166 ± 4 kJ mol^{-1}), confirming that the rDA reaction was easier to carry out than the DA reaction. It thus proved the quite low stability of the DA adduct in the surface of NPs, maybe due to the Brownian motion of the particles, stretching the bonds. Moreover, the transition state theory enabled the calculation of thermodynamic parameters related to the formation of the transition state during the rDA reaction (Figure S8): the enthalpy of activation was $\Delta H^{\neq}$ = 0.98 ± 0.05 kJ mol^{-1} and the entropy of activation was $\Delta S^{\neq}$ = 0.20 ± 0.02 kJ mol^{-1} K^{-1}. The positive value of $\Delta H^{\neq}$ confirmed that the rDA reaction was endothermic. The value of $\Delta S^{\neq}$ shows that few increases of disorder occurred the separation of NPs from each other's.

Then, the reversibility of the reaction was investigated for five cooling/heating cycles performed under the optimized conditions, *i.e.* at 298 K during 2 hrs for the DA reaction (cooling step) and at 323 K during 1 hr for the rDA reaction (heating step). After each step, the size of the system was characterized by DLS (Figure 5.b). After each cooling step, the size value was about 200 nm due to covalent aggregation of the NPs. It is also interesting to observe the size decrease, down to 20 nm, after each heating step, corresponding to the separation of NPs aggregates *via* the rDA reaction. The fact that several cycles could be carried out indicated that the nanoparticles' chemistry and shape were not altered. These results prove for the first time the perfect reversibility under mild conditions of the interfacial DA reaction in-between nanoparticles for at least five DA/rDA cycles.

Naked-eye observation and cryo-TEM images confirmed the previous results and proved that the polymer was not degraded during the heating step (Figure 6). Indeed, the formation of aggregates (around 80 nm) and the whitening of the solution first proved the formation of covalent bonds between FUR_120 and MAL_120 by interfacial DA reaction at 298 K (Figure 6.b) and the further observation of isolated nanoparticles and the transparent solution then proved the debonding of FUR_120 NPs and MAL_120 NPs *via* interfacial rDA reaction at 323 K in 1 hour (Figure 6.c).

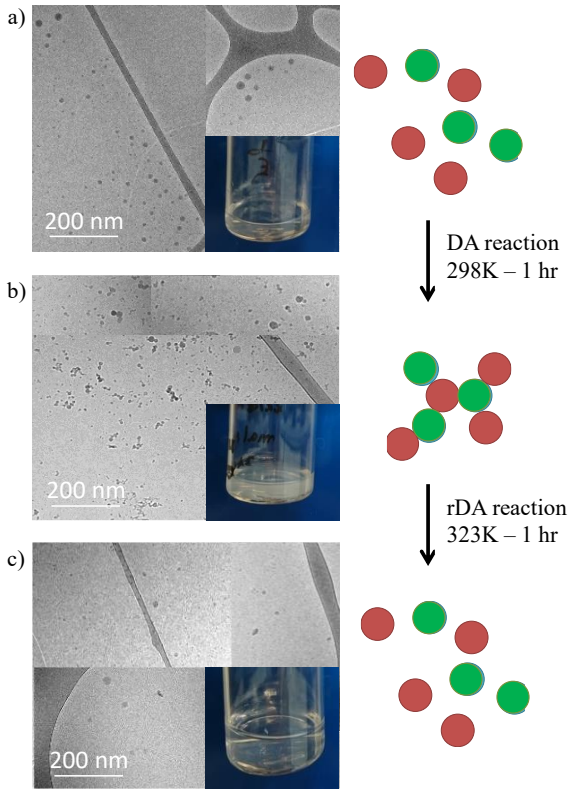

Figure 6. Cryo-TEM images, solution color and schematic illustration a) just after mixing FUR_120 and MAL_120 nanosuspensions (t = 0 min), b) after mixing FUR_120 and MAL_120 nanosuspensions at 298 K for 60 min and c) after heating (b) at 323 K for 1 hr. In the schematic illustration, FUR_120 NPs are represented as red dots and MAL_120 NPs are represented as green dots.

So, nanoparticles produced from furan-functionalized PLGA and maleimide-functionalized PLGA can be covalently bonded thanks to DA reaction at room temperature in less than 2 hrs and easily debonded thanks to rDA reaction at 323 K (reaction time: 1 hr).

IV. CONCLUSION

In this work, the interfacial Diels-Alder reaction as a way to reversibly bond two nanoparticles, produced from DA-reactive polymers, has been investigated. Assemblies made of maleimide- and furan-functionalized PLGA nanoparticles were obtained and their reversible aggregation was investigated, for the first time, under mild conditions (in water and with reaction temperatures under 373 K). The reactivity of these DA-reactive NPs' surfaces was then quantified by determining the kinetics and thermodynamic parameters (the activation energy of the reactions as well as the thermodynamic parameters associated to the transition states) of the interfacial DA and rDA reactions. A thorough understanding of interfacial reactivity between nanoparticles was consequently provided. The obtained values of activation energy of the DA reaction and of the thermodynamic parameters associated to the transition state were different from the one in solution because of the high mobility of the NPs, due to their Brownian motion, limiting the probability that two appropriately oriented reactive groups meet to conduct the cycloaddition. The study of the interfacial reactivity of the rDA reaction, done for the first time between particles, proved that this reaction was easier to carry out than the DA reaction. This effect was attributed to the limited stability of the DA adduct at the surface of NPs. This work has highlighted that confinement effects at the surface of NPs play a significant role on the interfacial DA and rDA reactivity.

The durable reversibility of the bonding/debonding process was ensured by good stability of the chemistry thanks to a moderate rDA temperature (323 K). As a conclusion, the results of this study open innovative perspectives for the design of new smart particles.

ACKNOWLEDGMENTS

The authors would like to thank Marc Schmutz, Catherine Foussat and Mélanie Legros for the access to the ICS characterization platforms. This work of the Interdisciplinary Institute HiFunMat, as part of the ITI 2021-2028 program of the University

of Strasbourg, CNRS and Inserm, was supported by IdEx Unistra (ANR-10-IDEX-0002) and SFRI (STRAT'US project, ANR-20-SFRI-0012) under the framework of the French Investments for the Future Program.

REFERENCES

[1] M. A. Cohen Stuart, W. T. S. Huck, J. Genzer, M. Müller, C. Ober, M. Stamm, G. B. Sukhorukov, I. Szleifer, V.V. Tsukruk, M. Urban, F. Winnik, S. Zauscher, I. Luzinov, S. Minko, Emerging applications of stimuli-responsive polymer materials. *Nature Mater* **2010**, *9*, 101–113.

[2] V. Amendola, M. Meneghetti, Self-Healing at the Nanoscale: Mechanisms and Key Concepts of Natural and Artificial Systems. *CRC Press*, **2011**.

[3] D. Limón, C. Jiménez-Newman, M. Rodrigues, A. González-Campo, D. B. Amabilino, A. C. Calpena, L. Pérez-García, Cationic supramolecular hydrogels for overcoming the skin barrier in drug delivery. *Chemistry Open* **2017**, *6* (4), 585–598.

[4] R. J. Wojtecki, M. A. Meador, S. J. Rowan, Using the dynamic bond to access macroscopically responsive structurally dynamic polymers. *Nat. Mater.* **2011**, *10* (1), 14–27.

[5] C. de las H. Alarcón, S. Pennadam, C. Alexander, Stimuli responsive polymers for biomedical applications. *Chem. Soc. Rev.* **2005**, *34* (3), 276–285.

[6] P. Theato, B. Sumerlin, K. R. O'Reilly, H. Thomas, Stimuli responsive materials. *Chem. Soc. Rev.* **2013**, *42* (17), 7055–7056.

[7] D. M. Lynn, M. M. Amiji, R. Langer, pH-responsive polymer microspheres: Rapid release of encapsulated material within the range of intracellular pH. *Angew. Chem.* **2001**, *113* (9), 1757–1760.

[8] T. Shimanouchi, S. Morita, H. Umakoshi, R. Kuboi, Stimuli-responsive separation of proteins using immobilized liposome chromatography. *J. Chromatogr. B. Biomed. Sci. App.* **2000**, *743* (1), 85–91.

[9] A. Phadke, C. Zhang, B. Arman, C. C. Hsu, R. A. Mashelkar, A. K. Lele, M. J. Tauber, G. Arya, S. Varghese, Rapid self-healing hydrogels. *Proc. Natl. Acad. Sci.* **2012**, *109* (12), 4383–4388.

[10] C. C. Peng, V. A. Abetz, A Simple Pathway toward Quantitative Modification of Polybutadiene: A New Approach to Thermoreversible Cross-Linking Rubber Comprising Supramolecular Hydrogen-Bonding Networks. *Macromolecules* **2005**, *38* (13), 5575–5580.

[11] Y. Chen, A. M. Kushner, G. A. Williams, Z. Guan, Multiphase design of autonomic self-healing thermoplastic elastomers. *Nat. Chem.* **2012**, *4* (6), 467–472.

[12] R. F. M. Lange, M. V. Gurp, E. W. Meijer, Hydrogen-bonded supramolecular polymer networks. *J. Polym. Sci. Part Polym. Chem.* **1999**, *37* (19), 3657–3670.

[13] D. Rongching, R. B. Stein, B. J. Andrews, K. B. James, M. Wieler, Application of tilt sensors in functional electrical stimulation. *IEEE Trans. Rehabil. Eng.* **1996**, *4* (2), 63–72.

[14] A. Pascual-Leone, D. Nguyet, L. G. Cohen, J. P. Brasil-Neto, A. Cammarota, M. Hallett, Modulation of muscle responses evoked by transcranial magnetic stimulation during the acquisition of new fine motor skills. *J. Neurophysiol.* **1995**, *74* (3), 1037–1045.

[15] M. B. Schneider, D. J. Mishelevich, Robotic apparatus for targeting and producing deep, focused transcranial magnetic stimulation. *US7520848B2*, **2009**.

[16] T. Manouras, M. Vamvakaki, Field responsive materials: photo-, electro-, magnetic-and ultrasound-sensitive polymers. *Polym. Chem.* **2017**, *8* (1), 74–96.

[17] H. Guo, N. Sanson, D. Hourdet, A. Marcellan, Thermoresponsive Toughening with Crack Bifurcation in Phase-Separated Hydrogels under Isochoric Conditions. *Adv. Mater.* **2016**, *28* (28), 5857–5864.

[18] F. Garcia, M. M. J. Smulders, Dynamic covalent polymers. *J. Polym. Sci. Part A: Polymer Chemistry*. **2016**, 54 (22), 3551-3577.

[19] P. Cordier, F. Tournilhac, C. Soulié-Ziakovic, L. Leibler, Self-healing and thermoreversible rubber from supramolecular assembly. *Nature* **2008**, *451* (7181), 977–980.

[20] M. J. Solomon, P. Varadan, Dynamic structure of thermoreversible colloidal gels of adhesive spheres. *Phys. Rev. E* **2001**, *63* (5), 051402.

[21] H. Otsuka, K. Aotani, Y. Higaki, Y. Amamoto, A. Takahara, Thermal reorganization and molecular weight control of dynamic covalent polymers containing alkoxyamines in their main chains. *Macromolecules* **2007**, *40* (5), 1429–1434.

[22] J. Kulis, C. A. Bell, A. S. Micallef, Z. Jia, M. J. Monteiro, Rapid, selective, and reversible nitroxide radical coupling (NRC) reactions at ambient temperature. *Macromolecules* **2009**, *42* (21), 8218–8227.

[23] N. Van Herck, F. E. Du Prez, Fast healing of polyurethane thermosets using reversible triazolinedione chemistry and shape-memory. *Macromolecules* **2018**, *51* (9), 3405–3414.

[24] O. Diels, K. Alder, Synthesen in der hydroaromatischen Reihe. *Justus Liebigs Annalen der Chemie*. **1928**, *460* (1), 98-122.

[25] A. Gandini, The application of the Diels-Alder reaction to polymer syntheses based on furan/maleimide reversible couplings. *Polimeros* **2005**, *15* (2).

[26] M. Tasdelen, Diels–Alder "click" reactions: recent applications in polymer and material science. *Polym. Chem.* **2011**, *2* (10), 2133–2145.

[27] T. Pauloehrl, G. Delaittre, V. Winkler, A. Welle, M. Bruns, H. G. Börner, A. M. Greiner, M. Bastmeyer, C. Barner-Kowollik, Adding Spatial Control to Click Chemistry: Phototriggered Diels–Alder Surface (Bio)functionalization at Ambient Temperature. *Angew. Chem. Internat. Ed.* **2011**, *51* (4), 1071-1074.

[28] W. Fan, W. Yan, Z. Xu, H. Ni, Formation mechanism of monodisperse, low molecular weight chitosan nanoparticles by ionic gelation technique. *Colloids Surf. B Biointerfaces* **2012**, *90*, 21–27.

[29] S. Khoee, P. M. Bakvand, Synthesis of dual-responsive Janus nanovehicle via PNIPAm modified SPIONs deposition on crosslinked chitosan microparticles and decrosslinking process in the core. *European Polymer Journal* **2019**, *114*, 411-425.

[30] M. Cao, Y. Wang, X. Hu, H. Gong, R. Li, H. Cox, J. Zhang, T. A. Waigh, H. Xu, J. R. Lu, Reversible Thermoresponsive Peptide-PNIPAM Hydrogels for Controlled Drug Delivery. *Biomacromolecules* **2019**, *20* (9), 3601–3610.

[31] L. Han, Y. Zhang, X. Lu, K. Wang, Z. Wang, H. Zhang, Polydopamine nanoparticles modulating stimuli-responsive PNIPAM hydrogels with cell/tissue adhesiveness. *ACS Appl. Mater. Interfaces* **2016**, *8* (42), 29088–29100.

[32] A. Saad, R. Mills, H. Wan, L. Ormsbee, D. Bhattacharyya, Thermoresponsive PNIPAm–PMMA-Functionalized PVDF Membranes with Reactive Fe–Pd Nanoparticles for PCB Degradation. *Ind. Eng. Chem. Res.* **2020**, *59* (38), 16614–16625.

[33] M. Vauthier, L. Jierry, M. L. Martinez Mendez, Y. M. Durst, J. B. Kelber, V. Roucoules, F. Bally-Le Gall, Interfacial Diels–Alder Reaction between Furan-Functionalized Polymer Coatings and Maleimide-Terminated Poly(ethylene glycol). *J. Phys. Chem. C.* **2019**. *123* (7), 4125-4132.

[34] M. Vauthier, L. Jierry, J. C. Oliveira, L. Hassouna, V. Roucoules, F. Bally-Le Gall, Interfacial thermoreversible chemistry on functional coatings: a focus on the Diels–Alder reaction. *Adv. Funct. Mater.* **2018**, *29* (10), 1806765.

[35] A. Gandini, D. Coelho, A. J. D. Silvestre, Reversible click chemistry at the service of macromolecular materials. Part 1: Kinetics of the Diels–Alder reaction applied to furan–maleimide model compounds and linear polymerizations. *Eur. Polym. J.* **2008**, *44* (12), 4029–4036.

[36] A. Gandini, The furan/maleimide Diels–Alder reaction: A versatile click–unclick tool in macromolecular synthesis. *Prog. Polym. Sci.* **2013**, *38* (1), 1–29.

[37] V. Froidevaux, M. Borne, E. Laborbe, R. Auvergne, A. Gandini, B. Boutevin, Study of the Diels–Alder and retro-Diels–Alder reaction between furan derivatives and maleimide for the creation of new materials. *RSC Adv.* **2015**, *5* (47), 37742–37754.

[38] G. Agrawal, R. Agrawal, Janus nanoparticles: Recent advances in their interfacial and biomedical applications. *ACS Appl. Nano Mater.* **2019**, *2* (4), 1738–1757.

[39] M. Vauthier, C. A. Serra, One-step production of polyelectrolyte nanoparticles. *Polym. Int*. **2021**, *70* (6), 860-865.

[40] F. Esmaeili, M. H. Ghahremani, S. N. Ostad, F. Atyabi, M. Seyedabadi, M. R. Malekshahi, M. Amini, R. Dinarvand, Folate-receptor-targeted delivery of docetaxel nanoparticles prepared by PLGA–PEG–folate conjugate. *J. Drug Target.* **2008**, *16* (5), 415–423.

[41] N. Anton, F. Bally, C. A. Serra, A. Ali, Y. Arntz, Y. Mely, M. Zhao, E. Marchioni, A. Jakhmola, T. F. Vandamme, A new microfluidic setup for precise control of the polymer nanoprecipitation process and lipophilic drug encapsulation. *Soft Matter.* **2012**, *8* (41), 10628-10635.

[42] S. Ding, N. Anton, T. F. Vandamme, C. A. Serra, Microfluidic nanoprecipitation systems for preparing pure drug or polymeric drug loaded nanoparticles: an overview. *Expert Opin. Drug Deliv.* **2016**, *13* (10), 1447–1460.

[43] M. Vauthier, M. Schmutz, C. A. Serra, One-step Elaboration of Janus Polymeric Nanoparticles: a Comparative Study of Different Emulsification Processes. *Coll. Surf. A: Physicochem. Eng. Aspects*. **2021**, 626, 127059.

[44] W. Yu, C. A. Serra, I. U. Khan, S. Ding, R. I. Gomez, M. Bouquey, R. Muller, Development of an Elongational-Flow Microprocess for the Production of Size-Controlled Nanoemulsions: Batch Operation. *Macromol. React. Eng.* **2017**, *11* (1), 1600024.

[45] I. Derényi, T. Vicsek, Cooperative transport of Brownian particles. *Phys. Rev. Lett.* **1995**, *75* (3), 374–377.

[46] J. Canadell, H. Fischer, G. D. With, R. A. T. M. van Benthem, Stereoisomeric effects in thermo-remendable polymer networks based on Diels–Alder crosslink reactions. *J. Polym. Sci. Part Polym. Chem.* **2010**, *48* (15), 3456–3467.

GRAPHICAL ABSTRACT